

RECONSTRUCTION OF THE SHAPE AND SURFACE IMPEDANCE FROM ACOUSTIC SCATTERING DATA FOR AN ARBITRARY CYLINDER*

J. J. LIU[†], G. NAKAMURA[‡], AND M. SINI[§]

Abstract. The inverse scattering for an obstacle $D \subset R^2$ with mixed boundary condition can be considered as a prototype for radar detection of complex obstacles with coated and noncoated parts of the boundary. We construct some indicator functions for this inverse problem using the far-field pattern directly, without the necessity of transforming the far field to the near field. Based on careful singularity analysis, these indicator functions enable us to reconstruct the shape of the obstacle and distinguish the coated from the noncoated part of the boundary. Moreover, an explicit representation formula for the surface impedance in the coated part of the boundary is also given. Our reconstruction scheme reveals that the coated part of the obstacle is less visible than the noncoated one, which corresponds to the physical fact that the coated boundary absorbs some part of the scattered wave. Numerics are presented for the reconstruction formulas, which show that both the boundary shape and the surface impedance in the coated part of the boundary can be reconstructed accurately. The theoretical reconstruction techniques proposed in this work can be applied in the practical 3-dimensional electromagnetic inverse scattering problems with promising numerical performance. Such problems are of great importance in the design of nondetectable obstacles.

Key words. inverse scattering, far field, impedance boundary, singularity analysis, numerics

AMS subject classifications. 35P25, 35R30, 78A45

DOI. 10.1137/060654220

Introduction and examples. Inverse scattering problems aim to identify some properties of an obstacle such as the boundary shape and type from the information contained in the scattered wave for given incident waves. Optimization techniques are well known for reconstructing the obstacle, up to some accuracy, by minimizing the objective functional for an unknown obstacle from given inversion input data by iteration procedures. However, it seems that a good initial guess is needed.

In recent years, some new inversion methods for the reconstruction of obstacle boundaries have been proposed. The common idea of these methods is the construction of some indicator functions from given inversion input data, which depend on some detecting point (a parameter) varying inside or outside the obstacle. When this point approaches the obstacle, these indicator functions blowup. The linear sampling method [7], the factorization method [16], and the singular sources method [21] construct the indicator functions from the far-field pattern directly, while the probe method [13, 14] constructs the indicator in terms of the near field. The near field

*Received by the editors March 13, 2006; accepted for publication (in revised form) January 17, 2007; published electronically May 14, 2007.

<http://www.siam.org/journals/siap/67-4/65422.html>

[†]Department of Mathematics, Southeast University, Nanjing, 210096, P.R. China (jjliu@seu.edu.cn). This author was supported by NSFC grant 10371018.

[‡]Department of Mathematics, Hokkaido University, Sapporo, 060-0810, Japan (gnaka@math.sci.hokudai.ac.jp). This author was partially supported by Grant-in-Aid for Scientific research (B)(2) (NO.14340038) of the Japan Society for Promotion of Science.

[§]Department of Mathematics, Yonsei University, Seoul, 120-749, Korea. Current address: Radon Institute for Computational and Applied Mathematics (RICAM), Austrian Academy of Sciences, Altenbergerstrasse 69, Linz, A-4040, Austria (mourad.sini@oeaw.ac.at). This author was supported by the IIRC of Kyung Hee University, Korea, via the SRC/ERC program of MOST/KOSEF (R11-2002-103).

can be obtained from the far field by some regularization procedures [21]. However, we can also state the natural version of the probe method directly from the far-field data, without reducing the far field to the near field; see [11]. For a review of these methods, the readers are referred to [22, 23], and for some relations between them, to [11, 20].

If the scattering is caused by multiple obstacles with different types of boundary or with mixed boundary condition, one should identify both the boundary shape, boundary type, and surface impedance. These kinds of problems come from some industry designs such as radar detection by electromagnetic wave scattering; see [10]. The obstacle is illuminated by an electromagnetic wave coming from an antenna. The wave is scattered by the obstacle and received by an antenna located in a different place. One of the objectives is to design the shape of the obstacle such that a reflected wave can be avoided or minimized in some directions. One possible approach to this goal is to introduce a coating on the surface of the obstacle or on some of its parts. This is motivated by the fact that reflections are minimized by applying such a surface coating. The surface coating is modeled by introducing an impedance boundary condition on a part or on the whole surface of the scatterer, which gives a relation between the electric and the magnetic field through a coefficient called surface impedance.

Due to this practical importance, the reconstruction of boundary impedance has been addressed by many authors. In [1], the authors construct the inhomogeneous boundary impedance for a cylinder obstacle with known shape using only one incident wave, assuming that the surface impedance is distributed along the whole boundary of the obstacle. In this case, the scattering of electromagnetic waves can be described by the 2-dimensional Helmholtz equation. We also refer to [17], where an optimization method is applied. After reducing the far field to the near field, a moment method is suggested in [6] to reconstruct the surface impedance approximately in the case of a completely coated obstacle, and the identification of different types of multiple obstacles is given in [5] in the case where on each obstacle we have one type of boundary condition.

The problem of whether a part of the surface of the obstacle is coated or not is important. Answering this question and reconstructing the surface impedance, in case of coating, from far-field measurements is our main object. In this work, we restrict ourselves to the acoustic wave scattering governed by a 2-dimensional Helmholtz equation, noticing that the 3-dimensional electromagnetic wave scattering in the cylinder case can be modeled by the 2-dimensional Helmholtz equation [8]. These issues were first considered in [2, 3] by the linear sampling method, where the authors simultaneously reconstruct the obstacle and compute the L^∞ -norm of the surface impedance. This can be used to answer the question of existence or absence of coating and to give the value of the surface impedance in case it is known to be constant.

Motivated by these last works, our aim is to give another way to consider these issues and give further information on the obstacle. We proceed by constructing some indicator functions giving a direct link between the far-field pattern and the physical parameters of the obstacle. More precisely, we establish pointwise formulas which enable us to detect the boundary of the scatterer and distinguish and recognize the coated and the noncoated parts of the obstacle surface. In addition, on the coated part of the obstacle, the indicator functions give explicitly the pointwise values of this surface impedance as a functional of the far fields. These types of results have been initiated in [19], where the theoretical justification of these formulas in

3-dimensional acoustic scattering is given. Since we need more singularity analysis in the 2-dimensional case than in 3-dimensional case, which is due to the use of a more singular point source, we give the theoretical justification of the steps where it is necessary, and refer to [19] for the rest of the proof. We would like to emphasize that we are reconstructing the obstacle, localizing the eventual coated part and reconstructing the surface impedance in one step, i.e., simultaneously; compare with [1, 2, 3, 5, 6, 17]. Also, since the analysis is done pointwise, we can also consider multiple obstacles and give similar results.

The validity of the theoretical reconstruction formula presented in this paper is also checked by numerical tests with satisfactory performances. We would like to mention the following observations from the numerics. The coated part of an obstacle with larger impedance is less visible than the other part in terms of the value of the indicator. This explains the practical motivation for introducing the coating, i.e., to avoid or perturb the detection of an obstacle by applying an absorbing boundary layer. On the other hand, for nonconvex obstacles with mixed boundary conditions, the inversion formulas proposed in this paper also generate a satisfactory reconstruction by combining different blowing-up criterion together. These reconstruction performances are supported by our numerical implementations given in the last section of this paper.

The rest of the paper is organized as follows. In section 1, we state the problem mathematically. In section 2, we present the results, which we prove in section 3. Section 4 is devoted to the numerical tests.

1. Statement of the problem. Let D be a bounded domain of R^2 such that $R^2 \setminus \bar{D}$ is connected. We assume that its boundary ∂D is of class C^2 and has the following form:

$$\partial D = \overline{\partial D_I} \cup \overline{\partial D_D}, \quad \partial D_I \cap \partial D_D = \emptyset,$$

where ∂D_D and ∂D_I are open surfaces in ∂D .

The propagation of time-harmonic acoustic fields in homogeneous cylinder media can be modeled by the Helmholtz equation

$$(1.1) \quad \Delta u + \kappa^2 u = 0 \quad \text{in } R^2 \setminus \bar{D},$$

where $\kappa > 0$ is the wave number. At the part ∂D_I of the obstacle boundary, we assume the total field u that satisfies the impedance boundary condition, while the part ∂D_D satisfies the Dirichlet boundary condition. That is,

$$(1.2) \quad \frac{\partial u}{\partial \nu} + i\kappa\sigma u = 0 \quad \text{on } \partial D_I$$

with some impedance function σ and

$$(1.3) \quad u = 0 \quad \text{on } \partial D_D,$$

where ν is the outward unit normal of ∂D . We assume that σ is a real valued Holder continuous function of order $\beta \in (0, 1]$ and has a uniform lower bound $\sigma_- > 0$ on ∂D_I . The part ∂D_I is referred to by the coated part of ∂D , and ∂D_D is the noncoated part.

For a given incident plane wave $u^i(x, d) = e^{i\kappa d \cdot x}$ with incident direction $d \in S^1$, where S^1 is a unit circle in R^2 , we look for a solution $u := u^i + u^s$ of (1.1), (1.2), and (1.3), where the scattered field u^s satisfies the Sommerfeld radiation condition

$$(1.4) \quad \lim_{r \rightarrow \infty} \sqrt{r} \left(\frac{\partial u^s}{\partial r} - i\kappa u^s \right) = 0$$

with $r = |x|$ and the limit is uniform for all directions $\hat{x} \in S^1$.

The mixed problem (1.1)–(1.4) is well posed. More generally, for $f \in H^{\frac{1}{2}}(\partial D_D)$ and $h \in H^{-\frac{1}{2}}(\partial D_I)$, there exists a unique solution of the mixed problem

$$(1.5) \quad \begin{cases} (\Delta + \kappa^2)u = 0 & \text{in } R^2 \setminus \overline{D}, \\ u = f & \text{on } \partial D_D, \\ \frac{\partial u}{\partial \nu} + i\kappa\sigma u = h & \text{on } \partial D_I, \\ \lim_{r \rightarrow \infty} \sqrt{r} \left(\frac{\partial u}{\partial r} - i\kappa u \right) = 0, \end{cases}$$

and the solution satisfies

$$(1.6) \quad \|u\|_{H^1(\Omega_R \cap (R^2 \setminus \overline{D}))} \leq C_R (\|f\|_{H^{1/2}(\partial D_D)} + \|h\|_{H^{-\frac{1}{2}}(\partial D_I)}),$$

where Ω_R is a disk of radius R and C_R is positive constant depending on R ; see [4] for more details.

It is well known (see [8]) that the scattered wave has the asymptotic behavior

$$(1.7) \quad u^s(x, d) = \frac{e^{i\kappa r}}{\sqrt{r}} u^\infty(\hat{x}, d) + O(r^{-3/2}), \quad r := |x| \rightarrow \infty,$$

where the function $u^\infty(\cdot, d)$ defined on S^1 is called the far field of the scattered wave u^s corresponding to incident direction d . We introduce a constant $\gamma_2 := \frac{e^{i\pi/4}}{\sqrt{8\pi\kappa}}$ and

$$\Phi(x, y) := \frac{i}{4} H_0^{(1)}(\kappa|x - y|), \quad x \neq y, x, y \in R^2,$$

the fundamental solution to the Helmholtz equation in R^2 , where $H_0^{(1)}$ is the Hankel function of the first kind of order zero. In this paper, we will consider the following.

Inverse scattering problem for an obstacle with mixed boundary type. Given $u^\infty(\cdot, \cdot)$ on $S^1 \times S^1$ for the scattering problem (1.1)–(1.4), reconstruct the shape of obstacle D , identify ∂D_I and ∂D_D , and reconstruct the surface impedance $\sigma(x)$ on ∂D_I .

2. Presentation of the results. It is well known also (see [8]) that the scattered field associated with the Herglotz incident field $v_g^i := v_g$ defined by

$$(2.1) \quad v_g(x) := \int_{S^1} e^{i\kappa x \cdot d} g(d) \, ds(d), \quad x \in R^2,$$

with $g \in L^2(S^1)$ is given by

$$(2.2) \quad v_g^s(x) := \int_{S^1} u^s(x, d) g(d) \, ds(d), \quad x \in R^2 \setminus D,$$

and its far field is

$$(2.3) \quad v_g^\infty(\hat{x}) := \int_{S^1} u^\infty(\hat{x}, d) g(d) \, ds(d), \quad \hat{x} \in S^1.$$

We will need the identity (see [8])

$$(2.4) \quad u^\infty(\hat{x}, d) = -\gamma_2 \int_{\partial D} \left\{ \frac{\partial u^s(y, d)}{\partial \nu} e^{-i\kappa \hat{x} \cdot y} - \frac{\partial e^{-i\kappa \hat{x} \cdot y}}{\partial \nu} u^s(y, d) \right\} ds(y)$$

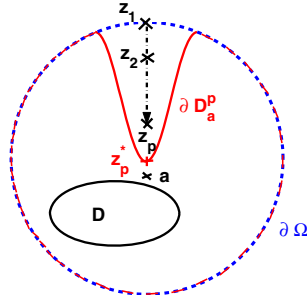


FIG. 2.1. Geometric configuration.

and the representation formula for the scattered wave $\Phi^s(\cdot, z)$ in $R^2 \setminus \bar{D}$ for the point source $\Phi(\cdot, z)$,

$$(2.5) \quad \Phi^s(x, z) = - \int_{\partial D} \left\{ \frac{\partial \Phi^s(y, z)}{\partial \nu(y)} \Phi(x, y) - \Phi^s(y, z) \frac{\partial \Phi(x, y)}{\partial \nu(y)} \right\} ds(y), \quad x, z \in R^2 \setminus \bar{D}.$$

Assume that $\bar{D} \subset \subset \Omega$ for some known Ω with smooth boundary. For $a \in \Omega \setminus D$, denote by $\{z_p\} \subset \Omega \setminus \bar{D}$ a sequence tending to a . For any z_p , set D_a^p a C^2 -regular domain such that $\bar{D} \subset D_a^p$ with $z_q \in \Omega \setminus \bar{D}_a^p$ for every $q = 1, 2, \dots, p$ and such that the Dirichlet interior problem on D_a^p for the Helmholtz equation is uniquely solvable; see Figure 2.1 for the configuration. In this case, the Herglotz wave operator \mathbb{H} defined from $L^2(S^1)$ to $L^2(\partial D_a^p)$ by

$$(2.6) \quad \mathbb{H}[g](x) := v_g(x) = \int_{S^1} e^{i\kappa x \cdot d} g(d) ds(d)$$

is injective compact with dense range; see [8]. Let z_p^* be a point on ∂D_a^p near z_p such that $z_p^* \rightarrow a$ as $z_p \rightarrow a$, as chosen in Figure 2.1. Denote by $\nu(z_p^*)$ the outward normal of ∂D_a^p at z_p^* . Now we consider the sequence of point sources $\Phi(\cdot, z_p)$. For every p fixed, we construct two density sequences $\{g_n^p\}$ and $\{f_m^p\}$ in $L^2(S^1)$ by the Tikhonov regularization such that

$$(2.7) \quad \|v_{g_n^p} - \Phi(\cdot, z_p)\|_{L^2(\partial D_a^p)} \rightarrow 0, \quad n \rightarrow \infty,$$

$$(2.8) \quad \left\| v_{f_m^p} - \frac{\partial}{\partial \nu(z_p^*)} \Phi(\cdot, z_p) \right\|_{L^2(\partial D_a^p)} \rightarrow 0, \quad m \rightarrow \infty,$$

where $\partial_{\nu(z_p^*)} \Phi(\cdot, z_p) := \nabla_x \Phi(x, z_p) \cdot \nu(z_p^*)$. Since both $v_{g_n^p}$ and $\Phi(\cdot, z_p)$ satisfy the same Helmholtz equation in D_a^p , (2.7) implies that

$$(2.9) \quad \|v_{g_n^p} - \Phi(\cdot, z_p)\|_{H^{\frac{1}{2}}(\partial D)} \rightarrow 0, \quad n \rightarrow \infty,$$

and

$$(2.10) \quad \left\| \frac{\partial}{\partial \nu} v_{g_n^p} - \frac{\partial}{\partial \nu} \Phi(\cdot, z_p) \right\|_{H^{-\frac{1}{2}}(\partial D)} \rightarrow 0, \quad n \rightarrow \infty.$$

Similarly, it follows from (2.8) that

$$(2.11) \quad \left\| v_{f_m^p} - \frac{\partial}{\partial \nu(z_p^*)} \Phi(\cdot, z_p) \right\|_{H^{\frac{1}{2}}(\partial D)} \rightarrow 0, \quad m \rightarrow \infty,$$

and

$$(2.12) \quad \left\| \frac{\partial}{\partial \nu} v_{f_m^p} - \frac{\partial}{\partial \nu} \left(\frac{\partial}{\partial \nu(z_p^*)} \Phi(\cdot, z_p) \right) \right\|_{H^{-\frac{1}{2}}(\partial D)} \rightarrow 0, \quad m \rightarrow \infty.$$

Multiplying (2.4) by $f_m^p(d)g_n^p(\hat{x})$ and integrating over $S^1 \times S^1$, we have

$$(2.13) \quad \begin{aligned} & - \int_{S^1} \int_{S^1} u^\infty(-\hat{x}, d) f_m^p(d) g_n^p(\hat{x}) ds(\hat{x}) ds(d) \\ &= \gamma_2 \int_{\partial D} \left\{ \int_{S^1} \frac{\partial u^s(y, d)}{\partial \nu} f_m^p(d) ds(d) \cdot \int_{S^1} e^{i\kappa \hat{x} \cdot y} g_n^p(\hat{x}) ds(\hat{x}) \right. \\ & \quad \left. - \int_{S^1} \frac{\partial e^{i\kappa \hat{x} \cdot y}}{\partial \nu} g_n^p(\hat{x}) ds(\hat{x}) \cdot \int_{S^1} u^s(y, d) f_m^p(d) ds(d) \right\} ds(y) \\ &= \gamma_2 \int_{\partial D} \left\{ \frac{\partial v_{f_m^p}^s}{\partial \nu}(y) v_{g_n^p}^i(y) - \frac{\partial v_{g_n^p}^i}{\partial \nu}(y) v_{f_m^p}^s(y) \right\} ds(y). \end{aligned}$$

From (2.9), (2.10), and (2.13), we have

$$(2.14) \quad \begin{aligned} & \lim_{n \rightarrow \infty} \int_{S^1} \int_{S^1} u^\infty(-\hat{x}, d) f_m^p(d) g_n^p(\hat{x}) ds(\hat{x}) ds(d) \\ &= \gamma_2 \int_{\partial D} \left\{ v_{f_m^p}^s \frac{\partial \Phi(y, z_p)}{\partial \nu(y)} - \frac{\partial v_{f_m^p}^s}{\partial \nu} \Phi(y, z_p) \right\} ds(y) \\ &= \gamma_2 v_{f_m^p}^s(z_p) \end{aligned}$$

from the Green formula, where $v_{f_m^p}^s(\cdot)$ is the scattered wave corresponding to incident wave $v_{f_m^p}^i(x) = \mathbb{H}[f_m^p](x)$.

Denote by $E^s(x, z_p)$ the scattered wave corresponding to the incident wave $\frac{\partial \Phi(x, z_p)}{\partial \nu(z_p^*)}$, which is well defined for every $x \in R^2 \setminus \bar{D}$. Then it follows from (2.11), (2.12), the well-posedness of the direct scattering problem, and the use of interior estimate that

$$(2.15) \quad E^s(x, z_p) = \lim_{m \rightarrow \infty} v_{f_m^p}^s(x), \quad x \in R^2 \setminus \bar{D}.$$

Finally, it follows from (2.14) that

$$(2.16) \quad \lim_{m \rightarrow \infty} \lim_{n \rightarrow \infty} \int_{S^1} \int_{S^1} u^\infty(-\hat{x}, d) f_m^p(d) g_n^p(\hat{x}) ds(\hat{x}) ds(d) = \gamma_2 E^s(z_p, z_p).$$

The reconstruction of ∂D as well as its surface impedance in the coating part can be established based on (2.16). For this purpose, an analysis of $E^s(x, z)$ near ∂D is the key point. We need the natural C^2 smoothness assumption on the regularity of ∂D . Precisely, for every point $a \in \partial D$, there exists a rigid transformation of coordinates under which the image of a is $\mathbf{0}$ and a function $f \in C^2(-r, r)$ such that

$$(2.17) \quad f(0) = \frac{df}{dx}(0) = 0, \quad D \cap B(\mathbf{0}, r) = \{(x, y) \in B(\mathbf{0}, r); y > f(x)\}$$

in terms of the new coordinates, where $B(\mathbf{0}, r)$ is the 2-dimensional ball of center $\mathbf{0}$ with radius r .

For the points $a \in \partial D$, we choose the sequence $\{z_p\}_{p \in \mathbb{N}}$ included in $C_{a, \theta}$, where $C_{a, \theta}$ is a cone with center a , angle $\theta \in [0, \frac{\pi}{2})$, and axis $\nu(a)$. The main theoretical result of this paper is as follows.

THEOREM 2.1. *Assume that the boundary ∂D is of class C^2 and that σ is a real valued Holder continuous function with positive lower bound. Then the boundary properties of the obstacle D can be identified by the following indicator functions:*

1. *The obstacle boundary ∂D can be constructed from the following property:*

$$(2.18) \quad \lim_{p \rightarrow \infty} \lim_{m, n \rightarrow \infty} \left| \operatorname{Re} \left[\gamma_2^{-1} \int_{S^1} \int_{S^1} u^\infty(-\hat{x}, d) f_m^p(d) g_n^p(\hat{x}) ds(\hat{x}) ds(d) \right] \right| = \begin{cases} +\infty, & a \in \partial D, \\ < +\infty, & a \in \Omega \setminus \bar{D}. \end{cases}$$

Precisely, we have the blowup rate

$$(2.19) \quad \lim_{m, n \rightarrow \infty} \operatorname{Re} \left[\gamma_2^{-1} \int_{S^1} \int_{S^1} u^\infty(-\hat{x}, d) f_m^p(d) g_n^p(\hat{x}) ds(\hat{x}) ds(d) \right] = \frac{\pm 1}{4\pi |(z_p - a) \cdot \nu(a)|} + O(|\ln |z_p - a||^2),$$

where $z_p := (z_{p,1}, z_{p,2})$ and $a = (a_1, a_2)$. The sign (+) is for $a \in \partial D_D$, while the sign (−) is for $a \in \partial D_I$.

2. *The coated and the noncoated parts of ∂D can also be distinguished from the following properties*

$$(2.20) \quad \lim_{p \rightarrow \infty} \lim_{m, n \rightarrow \infty} \frac{\operatorname{Im} \left[\gamma_2^{-1} \int_{S^1} \int_{S^1} u^\infty(-\hat{x}, d) f_m^p(d) g_n^p(\hat{x}) ds(\hat{x}) ds(d) \right]}{|\ln |(z_p - a) \cdot \nu(a)||^s} = \begin{cases} +\infty, & a \in \partial D_I, \\ 0, & a \in \partial D_D, \end{cases}$$

by choosing any fixed $s \in (0, 1)$.

3. *The impedance coefficient on ∂D_I can be detected by the following formula:*

$$(2.21) \quad \lim_{p \rightarrow \infty} \lim_{m, n \rightarrow \infty} \frac{\operatorname{Im} \left[\gamma_2^{-1} \int_{S^1} \int_{S^1} u^\infty(-\hat{x}, d) f_m^p(d) g_n^p(\hat{x}) ds(\hat{x}) ds(d) \right]}{|\ln |(z_p - a) \cdot \nu(a)||} = \frac{\kappa}{\pi} \sigma(a), \quad a \in \partial D_I.$$

REMARK 2.2. *The formula (2.18) is also true if f_m^p is replaced by g_n^p . That is, the singularity of $\Phi(x, z_p)$ is theoretically enough for identifying ∂D . However, as the blowup rate in this 2-dimensional case is of logarithmic order, it is not suitable to localize the obstacle clearly in the numerical experiments. For this reason, we introduced the density f_m^p , which is related to a stronger singularity $\frac{\partial}{\partial \nu(z_p^*)} \Phi(\cdot, z_p)$, to get a blowup rate of order $|z_p - a|^{-1}$. For the formulas (2.20) and (2.21), the stronger singularity of $\frac{\partial}{\partial \nu(z_p^*)} \Phi(\cdot, z_p)$ is necessary. Moreover, we can in fact use $\nu(a)$ instead of $\nu(z_p^*)$, since ∂D has been determined in terms of (2.18). The formula (2.19) can also be used to distinguish the coated part ∂D_I from the noncoated ∂D_I .*

REMARK 2.3. *Theorem 2.1 is stated for the case of a single obstacle. However, these results are still true for the multiple obstacle case with coated and noncoated parts.*

REMARK 2.4. *If $a \in D$, then the limit in (2.18) is conjectured to be ∞ ; see [11]. However, up to now, we do not have the full answer. The approach in [15] can be used to justify it in the case where the frequency κ is small enough.*

3. Proof of Theorem 2.1. For any given point $a \in \partial D$, we first take the rotation R_a and the translation M_a such that

$$R_a(\nu(a)) = (0, 1), \quad R_a(a) + M_a = \mathbf{0}$$

in the new coordinate system \tilde{x} . Under the transform $\tilde{x} := \mathbb{T}(x) := R_a(x) + M_a$, it follows that

$$\mathbb{T}(\nu(a)) = (0, 1), \quad \mathbb{T}(a) = \mathbf{0}.$$

Define $\tilde{\sigma}(\tilde{x}) := \sigma(x)$ and consider the following two problems in the coordinate $\tilde{x} = (\tilde{x}_1, \tilde{x}_2)$ for any given $\tilde{z} = (\tilde{z}_1, \tilde{z}_2) \in R_+^2$. We set $\tilde{w}_{\tilde{\sigma}(\mathbf{0})}^+(\tilde{x}, \tilde{z})$ and $\tilde{w}_D^+(\tilde{x}, \tilde{z})$ to be two functions satisfying

$$(3.1) \quad \begin{cases} \Delta \tilde{w}_{\tilde{\sigma}(\mathbf{0})}^+ = 0, & \tilde{x} \in R_+^2, \\ \left(\frac{\partial}{\partial \tilde{x}_2} \tilde{w}_{\tilde{\sigma}(\mathbf{0})}^+ + i\kappa \tilde{\sigma}(\mathbf{0}) \tilde{w}_{\tilde{\sigma}(\mathbf{0})}^+(\tilde{x}, \tilde{z}) \right) |_{\tilde{x}_2=0} = - \left(\frac{\partial}{\partial \tilde{x}_2} + i\kappa \tilde{\sigma}(\mathbf{0}) \right) \frac{\partial}{\partial \tilde{x}_2} \Gamma(\tilde{x}, \tilde{z}) |_{\tilde{x}_2=0}, \end{cases}$$

$$(3.2) \quad \begin{cases} \Delta \tilde{w}_D^+ = 0, & \tilde{x} \in R_+^2, \\ \tilde{w}_D^+(\tilde{x}, \tilde{z}) |_{\tilde{x}_2=0} = - \frac{\partial}{\partial \tilde{x}_2} \Gamma(\tilde{x}, \tilde{z}) |_{\tilde{x}_2=0}, \end{cases}$$

respectively, where $\Gamma(\tilde{x}, \tilde{z}) = \frac{1}{2\pi} \ln \frac{1}{|\tilde{x} - \tilde{z}|}$ and the subscript D in $\tilde{w}_D^+(\tilde{x}, \tilde{z})$ refers to the Dirichlet boundary condition in (3.2).

We give explicit solutions to these two problems in the following proposition.

PROPOSITION 3.1. *We have the explicit form of $w_{\tilde{\sigma}(\mathbf{0})}^+(\tilde{x}, \tilde{z})$,*

$$(3.3) \quad \tilde{w}_{\tilde{\sigma}(\mathbf{0})}^+(\tilde{x}, \tilde{z}) = \frac{1}{4\pi} \int_R e^{i(\tilde{x}_1 - \tilde{z}_1)\xi_1} e^{-(\tilde{x}_2 + \tilde{z}_2)|\xi_1|} \frac{|\xi_1| + i\kappa \tilde{\sigma}(\mathbf{0})}{|\xi_1| - i\kappa \tilde{\sigma}(\mathbf{0})} d\xi_1,$$

while $\tilde{w}_D^+(\tilde{x}, \tilde{z})$ has the form

$$(3.4) \quad \tilde{w}_D^+(\tilde{x}, \tilde{z}) = -\frac{1}{4\pi} \int_R e^{i(\tilde{x}_1 - \tilde{z}_1)\xi_1} e^{-(\tilde{x}_2 + \tilde{z}_2)|\xi_1|} d\xi_1.$$

This proposition can be proven by expressing

$$\tilde{w}_{\tilde{\sigma}(\mathbf{0})}^+(\tilde{x}, \tilde{z}) = (U_+[\tilde{x}_2]\phi_+)(\tilde{x}_1), \quad \tilde{w}_D^+(\tilde{x}, \tilde{z}) = (U_+[\tilde{x}_2]\phi_-)(\tilde{x}_1)$$

in R_+^2 with $(U_\pm[\tilde{x}_2]\phi)(\tilde{x}_1) := \frac{1}{2\pi} \int_R e^{i\tilde{x}_1\xi_1 \mp \tilde{x}_2|\xi_1|} \hat{\phi}(\xi_1, \tilde{z}) d\xi_1$ and computing the density functions ϕ_\pm from the boundary value problems (3.1), (3.2), where $\hat{\phi}$ is the 1-dimensional Fourier transform of ϕ ; see [19] for explicit computations.

Define

$$w_{\sigma(a)}^+(x, z) = \tilde{w}_{\tilde{\sigma}(\mathbf{0})}^+(\mathbb{T}x, \mathbb{T}z), \quad w_D^+(x, z) = \tilde{w}_D^+(\mathbb{T}x, \mathbb{T}z)$$

for $x, z \in R^2 \setminus \overline{D}$ near a , which is well defined by the definition of \mathbb{T} .

The next proposition gives the relation between $E^s(x, z)$ and $w_{\sigma(a)}^+(x, z), w_D^+(x, z)$ near the point a .

PROPOSITION 3.2. *If $a \in \partial D_I$, then there exist $\delta(a) > 0$ and $C > 0$ such that*

$$(3.5) \quad |\text{Im } E^s(x, z) - \text{Im } w_{\sigma(a)}^+(x, z)| \leq C \quad \text{for } (x, z) \in B_+(a, \delta(a)) \cap C_{a,\theta},$$

$$(3.6) \quad |\text{Re } E^s(x, z) - \text{Re } w_{\sigma(a)}^+(x, z)| \leq C |\ln |x - a|| \cdot |\ln |z_p - a||$$

for $(x, z) \in B_+(a, \delta(a)) \cap C_{a,\theta}$,

where $B_+(a, \delta(a)) := B(a, \delta(a)) \cap (R^2 \setminus D)$ and $B(a, \delta(a))$ is the ball of center a and radius $\delta(a)$.

Similarly, if $a \in \partial D_D$, we obtain (3.5) and (3.6) by replacing $w_{\sigma(a)}^+$ by w_D^+ .

REMARK 3.3. The estimate of $|\operatorname{Re} E^s(x, z) - \operatorname{Re} w_{\sigma(a)}^+(x, z)|$ is not optimal. We do not need the term $|\ln|x - a||$. The upper bound in (3.6) can be replaced by $C_\alpha|z - a|^{-\alpha}$ for any $\alpha > 0$, where C_α depends on α . But to prove Theorem 2.1 the estimate given in (3.6) is enough.

Now we can prove Theorem 2.1 based on these propositions.

Proof of Theorem 2.1.

Step A: It follows from Proposition 3.2 that

$$(3.7) \quad |\operatorname{Re} E^s(x, z_p) - \operatorname{Re} w^+(x, z_p)| \leq C \ln \frac{1}{|z_p - a|}$$

uniformly for all x, z_p near any fixed point $a \in \partial D$, where $w^+(z_p, z_p)$ may be $w_{\sigma(a)}^+(z_p, z_p)$ or $w_D^+(z_p, z_p)$, depending on the position of a . For $w^+(z_p, z_p) = w_D^+(z_p, z_p)$, it follows from (3.4) that

$$\operatorname{Re} w^+(z_p, z_p) = -\frac{1}{4\pi} \int_R e^{-2|z_{p,2} - a_2||\xi_1|} d\xi_1 = \frac{1}{4\pi|z_{p,2} - a_2|},$$

while for $w^+(z_p, z_p) = w_{\sigma(a)}^+(z_p, z_p)$ it holds from (3.3) that

$$\operatorname{Re} w^+(z_p, z_p) = \frac{1}{4\pi} \int_R e^{-2|z_{p,2} - a_2||\xi_1|} \frac{|\xi_1|^2 - \kappa^2 \sigma^2(a)}{|\xi_1|^2 + \kappa^2 \sigma^2(a)} d\xi_1 = -\frac{1}{4\pi|z_{p,2} - a_2|} + O(1),$$

where $z_p = (z_{p,1}, z_{p,2}) \rightarrow a = (a_1, a_2) \in \partial D$ as $p \rightarrow \infty$. The application of the above relations in (3.7) leads to (2.19) and then $\lim_{p \rightarrow \infty} |\operatorname{Re} E^s(z_p, z_p)| = +\infty$. Now (2.18) is proven for $a \in \partial D$.

Suppose that a is outside \bar{D} . We can construct z_p^*, z_p tending to a as we did for $a \in \partial D$. Recall that $E^s(x, z_p)$ satisfies

$$\begin{cases} (\Delta + \kappa^2)E^s(x, z_p) = 0 \text{ in } R^2 \setminus \bar{D}, \\ E^s(\cdot, z_p) = -\frac{\partial \Phi}{\partial \nu(z_p^*)}(x, z_p) \text{ on } \partial D_D, \\ (\frac{\partial}{\partial \nu} + i\kappa\sigma(x))E^s(x, z_p) = -(\partial_\nu + i\kappa\sigma(x))\frac{\partial \Phi}{\partial \nu(z_p^*)}(x, z_p) \text{ on } \partial D_I, \\ E^s(\cdot, z_p) \text{ satisfies the Sommerfeld radiation conditions,} \end{cases}$$

where $\nu(z_p^*)$ is the unit outward normal on ∂D_a^p at the point z_p^* . Hence the boundary condition is bounded with respect to x in $H^{1/2}(\partial D_D)$ and $H^{-\frac{1}{2}}(\partial D_I)$, respectively, for z_p^*, z_p near a . It follows from the well-posedness of the direct problem and interior estimates near a (i.e., away from ∂D) that $E^s(x, z_p)$, and then $E^s(z_p, z_p)$, is bounded.

Step B. Let $a \in \partial D_I$. From (3.3) we have

$$(3.8) \quad \tilde{w}_{\tilde{\sigma}(\mathbf{0})}^+(\tilde{z}, \tilde{z}) = \frac{1}{4\pi} \int_R e^{-2\tilde{z}_2|\xi_1|} \frac{|\xi_1| + i\kappa\tilde{\sigma}(\mathbf{0})}{|\xi_1| - i\kappa\tilde{\sigma}(\mathbf{0})} d\xi_1.$$

By taking the imaginary part and setting $\tilde{z} = (\tilde{z}_1, \tilde{z}_2) = R_a(z) + M_a$ for $z \in C(a, \theta)$, we get

$$(3.9) \quad \begin{aligned} \operatorname{Im}(4\pi w_{\sigma(a)}^+(z, z)) &= 4\kappa\sigma(a) \int_0^{+\infty} \frac{e^{-2(z-a)\cdot\nu(a)r}}{r^2 + \kappa^2\sigma(a)^2} dr \\ &= 4\kappa\sigma(a) \left[-\ln(\kappa\sigma(a)) - \ln((z-a)\cdot\nu(a)) \right. \\ &\quad \left. + 2 \int_0^{+\infty} \ln(r^2 + \kappa^2|(z-a)\cdot\nu(a)|^2\sigma^2(a))e^{-2r} dr \right], \end{aligned}$$

which leads to the first relation in (2.20) by dividing by $|\ln((z - a) \cdot \nu(a))|^s$ for $0 < (z - a) \cdot \nu(a) < 1$ with $0 < s < 1$ using (3.5) and (2.16). The representation (2.21) for $\sigma(a)$ can be gotten from the above relation by dividing by $|\ln((z - a) \cdot \nu(a))|$ for $0 < (z - a) \cdot \nu(a) < 1$.

Step C. Let $a \in \partial D_D$. Proposition 3.2 for $w_D^+(x, z)$ and (2.14) imply the second relation in (2.20), noticing the fact that $\text{Im}w_D^+(z, z) = 0$. \square

The rest of this section is devoted to the proof of Proposition 3.2. As we said in the introduction, in the 2-dimensional case, we need more singularity analysis than in [19]. This is due to the use of the more singular point source $\frac{\partial}{\partial \nu(z_p^*)}\Phi(\cdot, z_p)$. We give the detailed analysis and refer to [19] for the steps which do not need important changes.

3.1. Proof of Proposition 3.2. We give the proof for $a \in \partial D_I$. The proof for $a \in \partial D_D$ is similar.

Let $\tilde{E}^s(x, z_p)$ be the solution of

$$(3.10) \quad \begin{cases} (\Delta + \kappa^2)\tilde{E}^s(x, z_p) = 0 & \text{in } R^2 \setminus \bar{D}, \\ (\frac{\partial}{\partial \nu} + i\kappa\sigma(x))\tilde{E}^s(x, z_p) = -(\partial_\nu + i\sigma(x))\frac{\partial}{\partial \nu(z_p^*)}\Phi(x, z_p) & \text{on } \partial D, \\ \tilde{E}^s(\cdot, z) \text{ satisfies the Sommerfeld radiation condition.} \end{cases}$$

Hence $(E^s - \tilde{E}^s)(x, z_p)$ satisfies

$$(3.11) \quad \begin{cases} (\Delta + \kappa^2)(E^s - \tilde{E}^s)(x, z_p) = 0 & \text{in } R^2 \setminus \bar{D}, \\ (\frac{\partial}{\partial \nu} + i\kappa\sigma(x))(E^s - \tilde{E}^s)(x, z_p) = 0 & \text{on } \partial D_I, \\ (E^s - \tilde{E}^s)(\cdot, z_p) = -\frac{\partial}{\partial \nu(z_p^*)}\Phi(x, z_p) - \tilde{E}^s & \text{on } \partial D_D, \\ (E^s - \tilde{E}^s)(\cdot, z) \text{ satisfies the Sommerfeld radiation condition.} \end{cases}$$

We state $H_\sigma(x, z) := \tilde{E}(x, z) + \partial_{\nu(z_p^*)}\Phi(x, z)$. Hence H satisfies

$$(3.12) \quad \begin{cases} (\Delta + \kappa^2)H_\sigma(x, z) = -\nabla\delta(x, z) \cdot \nu(z_p^*) & \text{in } R^2 \setminus \bar{D}, \\ (\frac{\partial}{\partial \nu} + i\kappa\sigma(x))H_\sigma(x, z) = 0 & \text{on } \partial D, \\ H_\sigma(\cdot, z) \text{ satisfies the Sommerfeld radiation condition.} \end{cases}$$

We have the following estimates:

$$(3.13) \quad \begin{cases} |G_\sigma(x, z)| \leq c|\ln|x - z|| \\ |\nabla G_\sigma(x, z)| \leq c|x - z|^{-1} \\ |H_\sigma(x, z)| \leq c|x - z|^{-1} \\ |\nabla H_\sigma(x, z)| \leq c|x - z|^{-2} \end{cases} \text{ in } R^2 \setminus D, \text{ where } c \text{ is a positive constant.}$$

The justification of these properties can be derived following, for instance, the approach of [24] and [25] since an explicit form of a local fundamental solution for the half-space case can be derived as we did in Proposition 3.1. See also [18] and [12] for the case of elliptic problems with rough coefficients.

From these estimates, we deduce that $\tilde{E}(\cdot, z_p)$ and its derivatives are bounded for $x \in \partial D_D$ and z_p near $a \in \partial D_I$. The well-posedness of (3.11) implies that $(E^s - \tilde{E}^s)(\cdot, z_p)$ is bounded in $H_{loc}^1(R^2 \setminus \bar{D})$ for z_p near a . Introducing a cutoff function near the point a and using (3.11), we deduce that $(E^s - \tilde{E}^s)(\cdot, z_p)$ is bounded for x near ∂D_I and z_p near a .

This means that we can replace E^s by \tilde{E}^s in Proposition 3.2.

We introduce $w_\sigma^s(\cdot, z_p)$ as the solution of

$$(3.14) \quad \begin{cases} (\Delta + \kappa^2)w_\sigma^s(x, z_p) = 0 & \text{in } R^2 \setminus \overline{D}, \\ (\frac{\partial}{\partial \nu} + i\kappa\sigma(x))w_\sigma^s(x, z_p) = -(\frac{\partial}{\partial \nu} + i\sigma(x))\frac{\partial}{\partial \nu(a)}\Phi(\cdot, z_p) & \text{on } \partial D, \\ w_\sigma^s(\cdot, z) \text{ satisfies the Sommerfeld radiation condition,} \end{cases}$$

and denote by $w_{\sigma(a)}^s(\cdot, z_p)$ the solution of (3.14) replacing $\sigma(x)$ by $\sigma(a)$. Then we have the following result.

LEMMA 3.4. *There exist $\delta(a) > 0$ and $C(R) > 0$ such that*

$$|(\tilde{E}^s - w_\sigma^s)(x, z_p)| \leq C(R)|\ln d(x, \partial D)| \cdot |\ln d(z_p, \partial D)|,$$

$$|\text{Im}(\tilde{E}^s - w_\sigma^s)(x, z_p)| \leq C(R), \quad |(w_\sigma^s - w_{\sigma(a)}^s)(x, z_p)| \leq C(R)$$

for $z_p \in B(a, \delta(a)) \cap C_{a,\theta}$ and $x \in (R^2 \setminus D) \cap B(0, R)$, for any $R > 0$ fixed.

Let $w_{\sigma(a),\Phi}^s(\cdot, z)$ be the solution of

$$(3.15) \quad \begin{cases} (\Delta + \kappa^2)w_{\sigma(a),\Phi}^s(x, z) = 0 & \text{in } \Omega \setminus \overline{D}, \\ (\frac{\partial}{\partial \nu} + i\kappa\sigma(a))w_{\sigma(a),\Phi}^s(x, z) = -(\frac{\partial}{\partial \nu} + i\kappa\sigma(a))\frac{\partial}{\partial \nu(a)}\Phi(x, z_p) & \text{on } \partial D, \\ w_{\sigma(a),\Phi}^s(\cdot, z) = -\frac{\partial}{\partial \nu(a)}\Phi(x, z_p) & \text{on } \partial\Omega \end{cases}$$

and $w_{\sigma(a),\Gamma}^s(\cdot, z)$ be the solution of (3.15) replacing Φ by Γ . Then we have the following claim.

LEMMA 3.5. *There exists $C > 0$ such that*

$$|(w_{\sigma(a)}^s - w_{\sigma(a),\Phi}^s)(x, z)| \leq C, \quad |(w_{\sigma(a),\Phi}^s - w_{\sigma(a),\Gamma}^s)(x, z)| \leq C$$

for $z \in \Omega \setminus D$ near D and $x \in \Omega \setminus D$.

We define $w_{\sigma(a)}^{s,0}$ to be the solution of (3.15) replacing Φ by Γ and the Helmholtz equation by the Laplace equation. Then we have the next claim.

LEMMA 3.6. *There exists $C > 0$ such that $|(w_{\sigma(a),\Gamma}^s - w_{\sigma(a)}^{s,0})(x, z)| \leq C$, for $z \in \Omega \setminus D$ near D and $x \in \Omega \setminus D$.*

Finally, we have the next claim.

LEMMA 3.7. *There exist $C > 0, \delta(a) > 0$ such that*

1. $|\text{Im } w_{\sigma(a)}^{s,0} - \text{Im } w_{\sigma(a)}^+(x, z)| \leq C$ for $(x, z) \in B(a, \delta(a)) \cap C_{a,\theta}$;
2. $|\text{Re } w_{\sigma(a)}^{s,0} - \text{Re } w_{\sigma(a)}^+(x, z)| \leq C|\ln d(z_p, \partial D)|$ for $(x, z) \in B(a, \delta(a)) \cap C_{a,\theta}$.

By combining all the lemmas stated above, we end the proof of Proposition 3.2. \square

In the proofs of these lemmas we do not, in general, specify the interdependency of the constants appearing in the estimates. However, we distinguish the constants that do or do not depend on the angle θ .

Proof of Lemma 3.4. The function $\tilde{E}^s(x, z_p) - w_\sigma^s(x, z_p)$ satisfies

$$(3.16) \quad \begin{cases} (\Delta + \kappa^2)(\tilde{E}^s - w_\sigma^s)(x, z_p) = 0 & \text{in } R^2 \setminus \overline{D}, \\ (\frac{\partial}{\partial \nu} + i\kappa\sigma)(\tilde{E}^s - w_\sigma^s)(x, z_p) = -(\frac{\partial}{\partial \nu} + i\kappa\sigma)\nabla\Phi \cdot [\nu(z_p^*) - \nu(a)] & \text{on } \partial D, \\ (\tilde{E}^s - w_\sigma^s)(\cdot, z_p) \text{ satisfies the Sommerfeld radiation condition.} \end{cases}$$

We need the following lemma.

LEMMA 3.8. *We have the estimate*

$$|\nu(z_p^*) - \nu(a)| \leq C|z_p^* - a|$$

for z_p^* near a , where C is a positive constant.

Proof of Lemma 3.8. Take a point $b \in \partial\Omega$ and connect it to a by a C^3 smooth curve l such that $l(0) = a$, $l(1) = b$, $l(s) \in \Omega \setminus \overline{D}$ ($s \in (0, 1)$). By Theorem 7.1 of [11], there is a C^2 strict deformation family $\{D_a^{l(s)}\}$ of a and $\partial\Omega$. That is, each $\partial D_a^{l(s)}$ is C^2 diffeomorphic to the unit circle and $\{D_a^{l(s)}\}$ satisfies the following properties:

- (i) $a \in \partial D_a^{l(0)}$, $D \subset D_a^{l(0)} \subset \Omega$.
- (ii) $\partial D_a^{l(1)} = \partial\Omega$, $D_a^{l(s)} \subset D_a^{l(s')}$ ($0 \leq s < s' \leq 1$).
- (iii) l intersects $\partial D_a^{l(s)}$ at $l(s)$.
- (iv) $\partial D_a^{l(s)}$ depends C^2 smoothly on $s \in [0, 1]$.

For every $s \in [0, 1]$ we define $\nu(l(s))$ to be the unit normal of $\partial D_a^{l(s)}$ at $l(s)$. From (iv), the map $s \in [0, 1] \rightarrow \nu(l(s))$ is C^1 . Choosing l to be a one-to-one curve near a , we deduce that the map $l(s) \in l([0, 1]) \rightarrow \nu(l(s))$ is also C^1 near $l(0)$. Now let $\{s_p\} \subset [0, 1]$ be such that $s_p \rightarrow 0$ ($p \rightarrow \infty$) and let l be a C^3 smooth curve such that $z_p^* := l(s_p)$ and $\{z_p\}_{p \in \mathbb{N}} \subset l([0, 1])$. Since for every p , z_p and z_p^* are in $\Omega \setminus \overline{D}$, then we can always choose l such that $l(s) \in \Omega \setminus \overline{D}$, ($s \in [0, 1]$). We set $D_a^p := D_a^{l(s_p)}$. Hence the sequence $\nu(z_p^*)$ satisfies Lemma 3.8. \square

The function $\text{Im}(\tilde{E}^s - w_\sigma^s)$ satisfies

$$(3.17) \quad \begin{cases} (\Delta + \kappa^2)\text{Im}(\tilde{E}^s - w_\sigma^s)(x, z) = 0 & \text{in } R^2 \setminus \overline{D}, \\ \frac{\partial}{\partial \nu} \text{Im}(\tilde{E}^s - w_\sigma^s)(x, z) = [\kappa\sigma \text{Re}(\tilde{E}^s - w_\sigma^s) - [\frac{\partial}{\partial \nu} \text{Im} \nabla \Phi + \kappa\sigma \text{Re} \nabla \Phi] \cdot [\nu(z_p^*) - \nu(a)]](x, z) \\ \text{on } \partial D. \end{cases}$$

Hence we have

$$(3.18) \quad \begin{aligned} -\text{Im}(\tilde{E}^s - w_\sigma^s)(x, z_p) &= \int_{\partial D} F(y, z_p) G_N(y, x) ds(y) \\ &+ \int_{\partial B_R} \text{Im}(\tilde{E}^s - w_\sigma^s)(y, z_p) \frac{\partial}{\partial \nu} G_N(y, x) ds(y), \end{aligned}$$

where

$$F(x, z_p) := \kappa\sigma(x) \text{Re}(\tilde{E}^s - w_\sigma^s)(x, z) + \left[-\frac{\partial}{\partial \nu} \text{Im} \nabla \Phi - \kappa\sigma(x) \text{Re} \nabla \Phi \right] (x, z) \cdot [\nu(z_p^*) - \nu(a)],$$

and $G_N(x, y)$ is the Green's function of the problem given by the Helmholtz equation in $B_R \setminus \overline{D}$ with Neumann boundary condition on ∂D and Dirichlet boundary condition on ∂B_R . The normal ν is oriented outside $B \setminus \overline{D}$.

From (3.16), we have

$$-(\tilde{E}^s - w_\sigma^s)(x, z_p) = \int_{\partial D} G_\sigma(x, y) \left(\frac{\partial}{\partial \nu} + i\kappa\sigma(y) \right) [\nabla \Phi \cdot (\nu(z_p^*) - \nu(a))](y, z_p) ds(y).$$

Hence

$$|(\tilde{E}^s - w_\sigma^s)(x, z_p)| \leq c \int_{\partial D} (\ln|x - y|) |y - z_p|^{-2} |z_p^* - a| ds(y).$$

For $y \in \partial D$ and $z_p \in C_{a,\theta}$ we have the inequality $|z_p - a| \leq C(\theta)|z_p - y|$. Applying this inequality to z_p^* , enlarging θ if necessary, we have

$$(3.19) \quad |(\tilde{E}^s - w_\sigma^s)(x, z_p)| \leq c \int_{\partial D} (\ln|x - y|) |y - z_p|^{-1} ds(y)$$

since $|z_p^* - y| \leq |z_p - y|$, for $y \in \partial D$ and z_p near a . Hence for every $\alpha > 0$ there exists $C_\alpha > 0$ such that

$$|(\tilde{E}^s - w_\sigma^s)(x, z_p)| \leq C_\alpha |x - z_p|^{-\alpha}.$$

From the explicit form of Φ , we have $|\frac{\partial}{\partial \nu} \text{Im} \nabla \Phi(x, z_p)| \cdot |\nu(z_p^*) - \nu(a)| \leq c|x - z_p|^{-1} \cdot |z_p^* - a|$ and $\text{Re} \nabla \Phi(x, z_p) \cdot |\nu(z_p^*) - \nu(a)| \leq c|x - z_p|^{-1} |z_p^* - a|$. Hence $F(y, z_p) \leq C_\alpha |y - z_p|^{-\alpha}$ for $y \in \partial D$. Using the estimate $|G_N(x, y)| \leq C_\alpha \ln |x - y|$ and choosing $\alpha < 1$, we deduce from (3.18) that

$$|\text{Im}(\tilde{E}^s - w_\sigma^s)(x, z_p)| \leq C_\alpha.$$

We have the first estimate of Lemma 3.4 from (3.19), i.e.,

$$|(\tilde{E}^s - w_\sigma^s)(x, z_p)| \leq C \ln d(x, \partial D) \cdot |\ln d(z_p, \partial D)|.$$

Now consider the third estimate of Lemma 3.4. We set $R(x, z) := w_\sigma^s(x, z) - w_{\sigma(a)}^s(x, z)$. Then it satisfies

$$(3.20) \quad \begin{cases} (\Delta + \kappa^2)R(x, z) = 0 & \text{in } R^2 \setminus \bar{D}, \\ \frac{\partial R(x, z)}{\partial \nu} + i\kappa\sigma(a)R(x, z) = -i\kappa(\sigma(x) - \sigma(a))(w_\lambda^s(x, z) + \frac{\partial}{\partial \nu(a)}\Phi(x, z)) & \text{on } \partial D, \\ R(\cdot, z) \text{ satisfies the Sommerfeld radiation condition.} \end{cases}$$

From (3.20), we have the representation

$$(3.21) \quad R(x, z) = - \int_{\partial D} i\kappa(\sigma(y) - \sigma(a))G_{\sigma(a)}(y, x) \left(w_\sigma^s + \frac{\partial}{\partial \nu(a)}\Phi \right) (y, z) ds(y) \\ \text{for } (x, z) \in R^2 \setminus \bar{D}.$$

We define $K(x, z) := -(\frac{\partial}{\partial \nu} + i\kappa\sigma(x))\frac{\partial}{\partial \nu(a)}\Phi(x, z)$. From (3.14) we have the representation

$$w_\sigma^s(x, z) = \int_{\partial D} G_{\sigma(a)}(y, x)K(y, z)ds(y);$$

hence, due to the estimates of the Green's function $G_{\sigma(a)}(x, y)$ and $\Phi(x, y)$, we have

$$|w_\sigma^s(x, z)| \leq \int_{\partial D} |\ln(|y - x|)||z - y|^{-2} ds(y) \leq \frac{c}{|x - z|}.$$

From (3.21) and the Holder regularity of $\sigma(x)$, we deduce that

$$|R(x, z)| \leq c \int_{\partial D} |y - a|^\beta \ln(|y - x|)||z - y|^{-1} ds(y).$$

From the inequality $|y - a| \leq c(\theta)|y - z|$ for $y \in \partial D$ and $z \in C_{a,\theta} \cap B(a, \delta(a))$ we have

$$\frac{|y - a|^\beta}{|y - z|} \leq \frac{c(\theta)^\beta C}{|y - z|^{1-\beta}},$$

which implies

$$|R(x, z)| \leq \int_{\partial D} \frac{c(\theta)^\beta C |\ln |y - x||}{|y - z|^{1-\beta}} dy$$

and therefore $|R(x, z)| = O(1)$ for $x \in R^2 \setminus D$ and $z \in C_{a,\theta} \cap B(0, R)$. \square

Proof of Lemmas 3.5 and 3.6. Similarly to the proof of Lemma 3.4, these proofs are based on the use of integral representations and the pointwise estimates of the Green's functions of the corresponding problems. We omit the details. \square

Proof of Lemma 3.7. Since $w_{\sigma(a)}^{s,0}$ satisfies

$$(3.22) \quad \begin{cases} \Delta w_{\sigma(a)}^{s,0}(x, z) = 0 & \text{in } \Omega \setminus \bar{D}, \\ (\frac{\partial}{\partial \nu} + i\kappa\sigma(a))(w_{\sigma(a)}^{s,0}(\cdot, z)) = -(\frac{\partial}{\partial \nu} + i\kappa\sigma(a))\frac{\partial}{\partial \nu(a)}\Gamma & \text{on } \partial D, \\ w_{\sigma(a)}^{s,0}(\cdot, z) = -\frac{\partial}{\partial \nu(a)}(\Gamma) & \text{on } \partial\Omega, \end{cases}$$

then it is clear that $G_{\sigma(a)}^0 := w_{\sigma(a)}^{s,0}(x, y) + \partial_{\nu(a)}\Gamma(x, y)$ satisfies

$$(3.23) \quad \begin{cases} \Delta(G_{\sigma(a)}^0)(x, z) = -\frac{\partial}{\partial \nu(a)}\delta(x - y) & \text{in } \Omega \setminus \bar{D}, \\ (\frac{\partial}{\partial \nu} + i\kappa\sigma(a))(G_{\sigma(a)}^0)(\cdot, z) = 0 & \text{on } \partial D, \\ (G_{\sigma(a)}^0)(\cdot, z) = 0 & \text{on } \partial\Omega. \end{cases}$$

We can assume without loss of generality that $a = (0, 0)$ and $\nu(a) = (0, 1)$ by using the rigid transformation of coordinates $[R_a(\nu(a)) + M_a]$. Let $\xi = F(x)$ be the local change of variables

$$(3.24) \quad \xi_1 = x_1, \quad \xi_2 = x_2 - f(x_1),$$

where f is the function defined in the introduction. We have the following properties:

$$(3.25) \quad \begin{cases} c_1|x - z| \leq |F(x) - F(z)| \leq c_2|x - z|, \\ |F(x) - x| \leq c_3|x|^2, \\ |DF(x) - I| \leq c_4|x| \end{cases}$$

for x, z near the point a , where c_i ($i = 1, 2, 3, 4$) are positive constants, which is due to hypothesis on the regularity of ∂D .

Let x, z be points near a . From (3.23), we deduce that $\tilde{G}_{\sigma(a)}^0(\xi, \eta) = G_{\sigma(a)}^0(x, z)$ satisfies

$$(3.26) \quad \begin{cases} \nabla_\xi \cdot B(\xi)\nabla_\xi \tilde{G}_{\sigma(a)}^0 = -J^T(\xi)\nabla_\xi \delta(\xi - \eta) \cdot (0, 1) & \text{near } F(a), \\ |J^{-T}\nu|B(\xi)\nabla_\xi \tilde{G}_{\sigma(a)}^0 \cdot \tilde{\nu} + i\kappa\sigma(a)\tilde{G}_{\sigma(a)}^0 = 0 & \text{on } \partial R_+^2 \text{ near } F(a), \end{cases}$$

where $\xi := F(x)$ and $\eta := F(z)$, $B := JJ^T$ and $J := \frac{\partial \xi}{\partial x}(F^{-1}(\xi))$, and $\tilde{\nu} := (0, 1)$ is the unit normal to ∂R_+^2 . We denoted by J^{-T} the adjoint of J^{-1} . We have from (3.25) that

$$|J^T(\xi) - J^T(0)| \leq c|\xi|, \quad |B(\xi) - B(0)| \leq c|\xi|$$

and $J(0) = B(0) = I$.

We set $\Gamma_{\sigma(a)}(x, z) := (w_{\sigma(a)}^+ + \frac{\partial}{\partial x_2}\Gamma)(x, z)$ and write $\tilde{R}(\xi, \eta) := \tilde{G}_{\sigma(a)}^0(\xi, \eta) - \Gamma_{\sigma(a)}(\xi, \eta)$. Then the function $\tilde{R}(\cdot, \eta)$ satisfies

$$(3.27) \quad \begin{cases} \nabla_\xi \cdot B(\xi)\nabla_\xi \tilde{R} = \nabla_\xi \cdot (I - B)\nabla_\xi \Gamma_{\sigma(a)} + (I - J^T(\xi))\nabla_\xi \delta(\xi - \eta) \cdot (0, 1), \\ B(\xi)\nabla_\xi \tilde{R} \cdot \tilde{\nu} + i\kappa\sigma(a)\tilde{R} = (I - B)\nabla_\xi \Gamma_{\sigma(a)} \cdot \tilde{\nu} + i\kappa\sigma(a)(1 - |J^{-T}\nu|^{-1})\tilde{R}, \end{cases}$$

where the first relation holds in R_+^2 near $F(a)$, while the second one is satisfied on ∂R_+^2 near $F(a)$.

We remark that $(I - J^T(\xi))$ is equal to the matrix given by the two line vectors $(0, -f(\xi))$ and $(0, 0)$. Hence we have

$$(I - J^T(\xi))\nabla_\xi \text{Im}\Gamma_{\sigma(a)}(\xi, \eta) \cdot (0, 1) = 0.$$

With this remark, the problem (3.27) is exactly the one studied in [19]. We write $\partial B_r^+ = S_r \cup S_r^c$ with $S_r := \partial B_r^+ \cap \partial F(D)$. Arguing as in [19], we obtain the estimate

$$|\text{Im } \tilde{R}(\xi, \eta)| < c \quad \text{for } \xi \in S_r \text{ and } \eta \in C_{F(a),\theta}$$

and

$$|\text{Re } \tilde{R}(\xi, \eta)| < c |\ln |\xi - \eta|| \quad \text{for } \xi \in S_r \text{ and } \eta \in C_{F(a),\theta}.$$

We go back to $R(x, z) := G_{\sigma(a)}^0(x, z) - \Gamma_{\sigma(a)}(x, z)$. We have

$$R(x, z) = G_{\sigma(a)}^0(x, z) - \Gamma_{\sigma(a)}(F(x), F(z)) + \Gamma_{\sigma(a)}(F(x), F(z)) - \Gamma_{\sigma(a)}(x, z),$$

which can be rewritten as

$$(3.28) \quad \begin{aligned} R(x, z) &= \tilde{R}(F(x), F(z)) + [\Gamma_{\sigma(a)}(F(x), F(z)) - \Gamma_{\sigma(a)}(F(x), z)] \\ &\quad + [\Gamma_{\sigma(a)}(F(x), z) - \Gamma_{\sigma(a)}(x, z)]. \end{aligned}$$

By the same argument as in [19], we end up with the estimate

$$(3.29) \quad |\text{Im } R(x, z)| \leq c(\theta)$$

for $x \in B(a, \delta(a))$ such that $F(x) \in S_r$ and $z \in C_{a,\theta} \cap B(a, \delta(a))$.

For $z \in C_{a,\theta} \cap B(a, \frac{\delta(a)}{2})$ and $x \in [\partial B(a, \delta(a))] \cap R^2 \setminus \bar{D}$, we have

$$(3.30) \quad |\text{Im } R(x, z)| \leq c$$

with some positive constant c , because $C_{a,\theta} \cap B(a, \frac{\delta(a)}{2})$ and $[\partial B(a, \delta(a))] \cap R^2 \setminus \bar{D}$ are separated sets. Since in $B(a, \delta(a)) \cap (R^2 \setminus \bar{D})$, we have $\Delta_x \text{Im } R(x, z) = 0$; then, using (3.29) and (3.30), we have $|\text{Im } R(x, z)| \leq c(\theta)$ for $x \in [R^2 \setminus D] \cap B(a, \delta(a))$ and $z \in C_{a,\theta} \cap B(a, \frac{\delta(a)}{2})$, by the maximum principle.

Similarly we have $|\text{Re}R(x, z)| \leq C |\ln |x - z||$ for $x \in B(a, \delta(a))$ such that $F(x) \in S_r$ and $z \in C_{a,\theta} \cap B(a, \delta(a))$. Hence $|\text{Re}R(x, z)| \leq C |\ln d(z, \partial D)|$ for $x \in B(a, \delta(a))$ such that $F(x) \in S_r$ and $z \in C_{a,\theta} \cap B(a, \delta(a))$, which is the counterpart of (3.30) for $\text{Re}\tilde{R}$. The rest of the proof is the same as that for the imaginary part. \square

4. Numerical tests. In this section, we consider two reconstruction model problems for numerical tests based on Theorem 2.1. In the first model we take the obstacle to be a disc, and on its whole boundary we impose the impedance boundary condition. The purpose of considering such a model is to show the influence of wave number κ and singularity strength on the inversion scheme. In the second model, we consider a nonconvex obstacle with mixed boundary conditions. We check our inversion formulas fully, especially for the identification of a different type of boundary. Also we show the effect of the nonconvex part on the inversion performance.

In the reconstruction scheme, the approximation of $\Phi(x, z_p)$ and $\Phi_{\nu(a)}(x, z_p)$ by the Herglotz wave function plays a key role. To do this, we need to construct the approximate domain D_a^p in the way mentioned in section 2. Then its density functions

can be determined by the standard argument of a minimum norm solution of the integral equation of the first kind. In this way the numerators in (2.18), (2.20), and (2.21) can be computed for every sequence of points $(z_p)_{p \in \mathbb{N}}$ approaching ∂D in terms of the far-field pattern.

In testing our inversion scheme, we simulate the inversion input data (far-field pattern) by solving the direct problem using the combined single- and double-layer potential method; see [8] and [9].

In subsections 4.1 and 4.2, we consider the first model, while subsection 4.3 is dedicated to a nonconvex obstacle with mixed boundary conditions, from which we can test our theoretical results.

4.1. Reconstruction of ∂D . For the numerical test we take $\partial D = \{x = (x_1(t), x_2(t)) = 1.2(\cos t, \sin t) : t \in [0, 2\pi]\}$. We can construct D_a^p in a special way by

$$\partial D_a^p = \{(\tilde{x}_1(t), \tilde{x}_2(t)) = (1.2 + \delta_0(p))(\cos t, \sin t) : t \in [0, 2\pi]\}$$

and take $z_p = (\tilde{x}_1(t_0), \tilde{x}_2(t_0)) + \delta_1(p)(\cos t_0, \sin t_0)$ outside of \overline{D}_a^p for $a = 1.2(\cos t_0, \sin t_0)$ in ∂D . The smallness of $\delta_1(p)$ determines the singularity of $\Phi(x, z_p), \Phi_{\nu(a)}(x, z_p)$ on ∂D_a^p near z_p .

Example 1. Construction of ∂D with unknown impedance $\sigma(x)$ for given far-field data.

It follows from the first point of Theorem 2.1 that the boundary ∂D can be reconstructed from the blowup behavior of the approximate values of the indicator function:

$$(4.1) \quad I_{m,n}(z_p) \approx \left(\frac{\pi}{N}\right)^2 \left| \sum_{i,j=1}^{2N-1} \operatorname{Re}(\gamma_2^{-1} U^\infty(i,j) F_m^p(j) G_m^p(i)) \right|$$

for large m, n , where $G_n^p(i) := g_n^p(\hat{x}_i)$, $F_m^p(j) := f_m^p(\hat{d}_j)$, and $U^\infty(i, j)$ represents $u^\infty(-\hat{x}_i, d_j)$.

Therefore, we can test the numerical performance of this formula by taking z_p approaching ∂D . If $I_{m,n}(z_p)$ is greater than some a priori given large value, for fixed m, n large enough, we consider z_p to be almost in ∂D . Notice that only the singularity in $\Phi_{\nu(z_p)}(x, z_p)$ is needed in this procedure; we do not need the boundary ∂D .

In our numerical implementations, we take $\kappa = 0.6$, $N = 32$ and keep the singularity of $\Phi(\cdot, z_p)$ unchanged near ∂D_a^p by fixing $\delta_1 = 0.015$. When z_p approaches ∂D by decreasing δ_0 from different directions t_0 , we get different values of $I_{m,n}(z_p)$. We choose the same constant CB as the criterion for the blowing-up of the indicator $I_{m,n}(z_p(t_0))$ at different direction t_0 . That is, we choose $z_p(t_0)$ as the approximation of the point $a \in \partial D$ in the direction t_0 when $I_{m,n}(z_p(t_0))$ is larger than CB . Then the constructed approximate position of ∂D is given by interpolating those points. In this way, we can draw the approximate shape of ∂D by choosing all directions t_0 using the same given CB . As obtained in the theoretical result, the larger the value CB is, the better the approximation of ∂D should be.

Consider the boundary reconstruction problem with nonconstant impedance

$$\sigma(x) = \frac{2 + x_1 x_2}{(3 + x_2)^2}, \quad x \in \partial D.$$

Under this configuration, the reconstructions for different blowup criteria are shown in Figure 4.1(left), while the distribution of indicator value is given in the right panel.

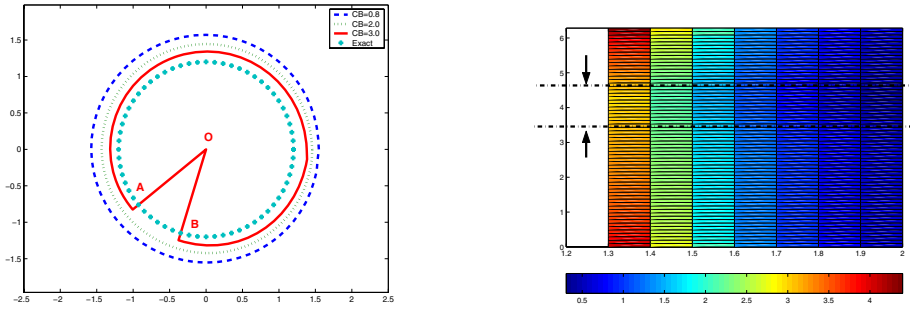


FIG. 4.1. Reconstruction of ∂D for variable impedance with $\kappa = 0.6$ with different blowup constants CB ; the values of the indicator are small in the directions corresponding to large impedance.

There is an interesting phenomenon in the numerics. For a reasonable indicator value $CB = 2$, we can see the whole rough shape of ∂D . However, for larger values, i.e., $CB = 3$, most of the part of ∂D can be seen with more satisfactory accuracy, but some part, i.e., (\widehat{AB}) , is not visible. In this part the indicator value is less than 3 (but, of course, bigger than 2). This numerical performance is closely related to the impedance distribution in ∂D . It can be seen from the right-hand part of Figure 4.1 that the indicator value is obviously smaller in the narrow domain at each radius layer. Therefore as r decreases, the part of ∂D related to these angles cannot be detected with the same accuracy. Considering the distribution of boundary impedance, this part corresponds to $\sigma(x)$ with large value, so it cannot be seen as clearly as the other part by using the same criterion values CB . This may be explained by the fact that the scattered wave along these directions will be much absorbed. Another, but related, reason is the property (2.19), i.e.,

$$\lim_{m,n \rightarrow \infty} \operatorname{Re} \left[\gamma_2^{-1} \int_{S^1} \int_{S^1} u^\infty(-\hat{x}, d) f_m^p(d) g_n^p(\hat{x}) ds(\hat{x}) ds(d) \right] = \frac{\pm 1}{4\pi |(z_p - a) \cdot \nu(a)|} + O(|\ln |z_p - a||),$$

where $O(|\ln |z_p - a||)$ may be large if σ is large near the point a . Hence numerically the second term can weaken the blowup of the first term.

Physically, this is the reason why we introduce the coated part of an obstacle, i.e., to avoid or perturb the detection of the obstacle.

The other special property of this example is that the whole boundary shape can be reconstructed well using only one blowup criterion CB . This comes from the special geometric shape and the fact that we have a complete impedance boundary condition. However, in the case of general problems, as for a nonconvex obstacle, with a mixed boundary condition we need to use multiple blowup values to get a satisfactory reconstruction; see subsection 4.3.

4.2. Reconstruction of $\sigma(x)$ for known ∂D . For a given $a \in \partial D$, we take $z_p \in \mathbb{R}^2 \setminus \overline{D}_a^p$ with $D \subset\subset D_a^p$.

By the theoretical result given in (2.21), the approximate formula for $\sigma(a)$ is

$$(4.2) \quad \frac{\kappa}{\pi} \sigma(a) \approx \frac{1}{|\ln((z_p - a) \cdot \nu(a))|} \left(\frac{\pi}{n}\right)^2 \sum_{i,j=1}^{2n-1} \operatorname{Im} (\gamma_2^{-1} U^\infty(i, j) F_m^p(j) G_n^p(i))$$

for large m, n and small $|z_p - a|$.

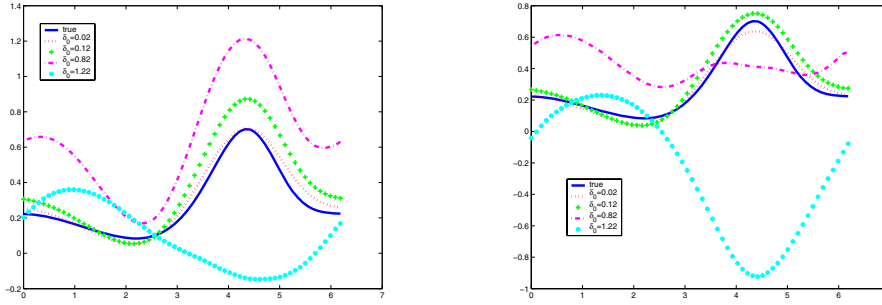


FIG. 4.2. Reconstruction of $\sigma(x) = \frac{2+x_1x_2}{(3+x_2)^2}$ for $\delta_0 = 1.22, 0.82, 0.12, 0.02$ with two different wave numbers $\kappa = 0.6$ (left) and $\kappa = 0.7$ (right), where we fix $\delta_1 = 0.015$.

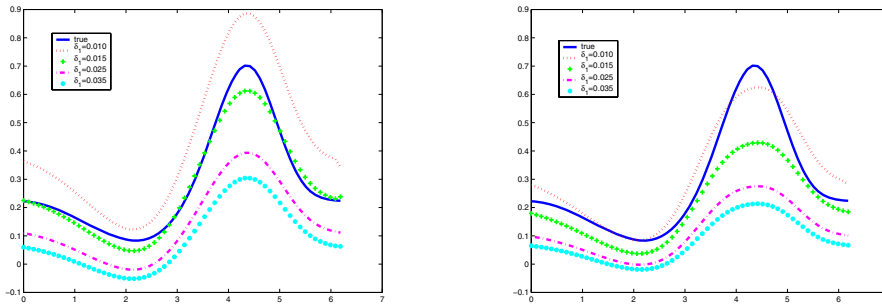


FIG. 4.3. Reconstruction of $\sigma(x) = \frac{2+x_1x_2}{(3+x_2)^2}$ for $\delta_1 = 0.010, 0.015, 0.025, 0.035$ with two different wave numbers $\kappa = 0.6$ (left) and $\kappa = 1.0$ (right), where we fix $\delta_0 = 0.002$.

Example 2. Consider the variable impedance distribution given in Example 1.

We take $n = 32$. First, let us keep the singularity unchanged by fixing δ_1 and shrink the radius of ∂D_a^p such that $z_p \rightarrow a \in \partial D$. The computed values of $\sigma(x(t))$ with fixed $\delta_1 = 0.015$ and different $\delta_0 = 1.22, 0.82, 0.12, 0.02$ for two wave numbers $\kappa = 0.6, \kappa = 0.7$ are shown in Figure 4.2. It can be seen from this figure that when $\delta_0 \rightarrow 0$ ($\delta_0 = 0.02$), the reconstruction results are satisfactory for both wave numbers.

It is interesting to see that when δ_0 is large enough ($\delta_0 = 1.22$), the reconstruction is invalid, even if here we use a strong singularity $\delta_1 = 0.015$. This is reasonable since the approximation to the strong singularity of the fundamental solution contains much error.

Finally, we fix ∂D_a^p near ∂D and take z_p tending to ∂D_a^p . In our configuration, this means $\delta_1 \rightarrow 0$ for fixed small δ_0 . The tests with $\delta_0 = 0.002$ for two wave numbers $\kappa = 0.6, 1.0$ at different $\delta_1 = 0.025, 0.020, 0.015, 0.010$ are given in Figure 4.3, which shows the influence of the singularity. It can be seen that the approximation is sensitive to the wave number κ . The reason is that we ignore the remaining term $C/|\ln |(z_p - a) \cdot \nu(a)||$, where the constant C comes from (3.5). Theoretically, this term tends to 0 as $z_p \rightarrow a$. However, this procedure causes a difficulty in approximating the fundamental solution. We expect that the constant C becomes large as κ becomes small. This is naturally related to the following relation, in the 2-dimensional case, between the fundamental solution to the Helmholtz and Laplace equations:

$$H_0^{(1)}(\kappa|x - y|) = -\frac{1}{2\pi} \ln(|x - y|) - \ln \kappa + O(1)$$

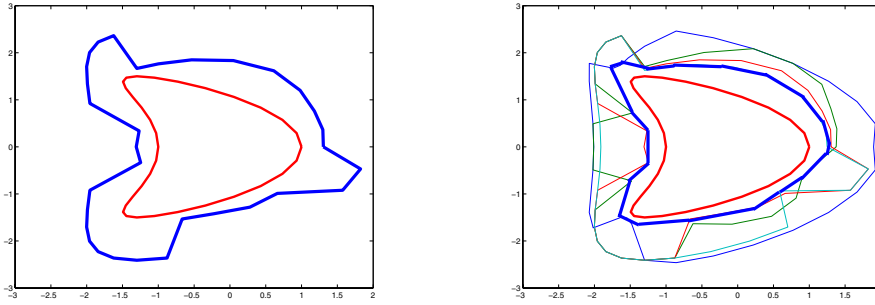


FIG. 4.4. Reconstruction of ∂D with $CB = 3.0$ (left) and four CB s (right) by concave-hull.

locally for $x, y \in R^2$ and κ small enough; see [8]. This implies that the difference between the fundamental solution behaves as $\ln \kappa$. So the constant C should have a similar behavior with respect to κ . These remarks on the dependency on wave number κ are also observed in the tests for detecting ∂D . However, we think that this is just a 2-dimensional phenomenon.

4.3. Reconstruction of an obstacle with mixed-type boundary. Since the main advantage of our inversion method is its ability to identify the full complex obstacle simultaneously, here we consider the numerical behavior of our inversion method acting on a nonconvex obstacle with mixed boundary condition.

Example 3. Consider a nonconvex obstacle D with the boundary

$$\partial D = \{x : x(t) = (x_1(t), x_2(t)) = (\cos t + 0.65 \cos 2t - 0.65, 1.5 \sin t), t \in [0, 2\pi]\}.$$

Let ∂D be composed of sound-soft part ∂D_D for $t \in [0, 1.42\pi]$, and impedance part ∂D_I for $t \in [1.42\pi, 2\pi]$. In ∂D_I , we assume the impedance coefficient $\sigma(x(t)) \equiv 3$.

We also choose ∂D_a^p and z_p in a special way. For two small constants $\delta_0, \delta_1 > 0$, we take

$$(4.3) \quad \begin{cases} \partial D_a^p = \{y(t) := x(t) + \delta_0 \times (\cos t, \sin t) : x(t) \in \partial D, t \in [0, 2\pi]\}, \\ z_p(t) = y(t) + \delta_1 \times (\cos t, \sin t) \quad \text{for } t \in [0, 2\pi]. \end{cases}$$

In terms of Theorem 2.1, the inversion schemes contain the following three steps:

Step 1. Identify the location of ∂D using (2.18);

Step 2. Distinguish the different parts of ∂D in terms of (2.20);

Step 3. Reconstruct $\sigma(x)$ in ∂D_I from (2.21).

We present the numerical results with fixed wave number $\kappa = 0.9$ and $\delta_1 = 0.01$.

Step 1. we take $n = 16$ and decrease $\delta_0 = l \times 0.05$ by taking l from 20 to 2. The indicator values in (2.18) for ∂D are computed for $z_p(t)$ and ∂D_a^p specified here for every direction t_j and different δ_0 . Then we draw the contour line to obtain an approximation of ∂D . As for Examples 1 and 2, we choose some appropriate value CB for the stopping rule of l . In the case when the indicator is always less than CB in some direction, we take z_p for the initial guess (the largest l) as an approximate location of points in ∂D .

In this case, the situation is different from the examples given in the previous subsections; the reconstruction of the boundary using only one blowup value CB is not sufficient. See the left-hand picture in Figure 4.4 for the reconstruction of $CB = 3.0$, where the kite-shape in red color is the exact obstacle. Enlarging CB

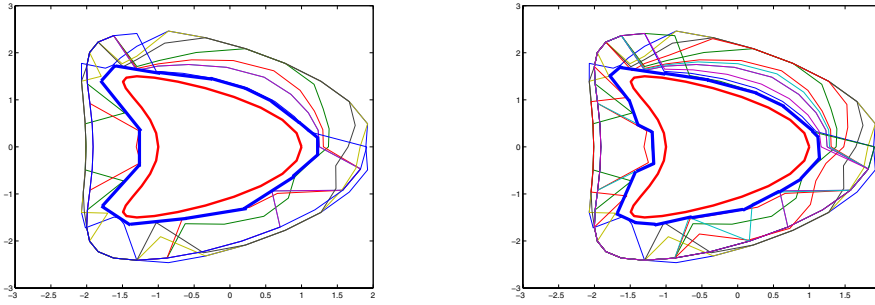


FIG. 4.5. Reconstruction of ∂D by concave-hull using eight CB s (left) and twelve CB s (right).

can improve the reconstruction along some directions, but the approximation to the whole boundary is still not satisfactory. The reason for this phenomenon is that our theoretical results do not guarantee the uniform blowup property for all directions.

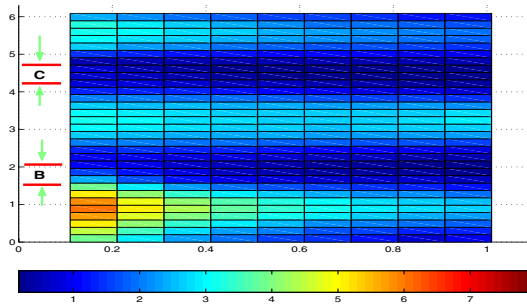


FIG. 4.6. The indicator values for boundary shape.

To overcome this difficulty and apply our reconstruction formula, we propose to combine the reconstruction results for different CB together and take the concave hull. Then ∂D can be approximated very well; see Figure 4.4, where we compare the shape given by using one CB only and the one obtained by using four CB values. In Figure 4.5, we show the reconstruction results by using eight and twelve CB values. Precisely, the reconstructions in Figures 4.4 and 4.5 correspond to the following CB values:

Figure 4.4 (right): four values— $CB = 0.8, 2.5, 3.0, 3.5$;

Figure 4.5 (left): eight values— $CB = 0.8, 2.5, 3.0, 3.5, 1.2, 1.5, 5.5, 6.5$;

Figure 4.5 (right): twelve values— $CB = 0.8, 2.5, 3.0, 3.5, 1.2, 1.5, 5.5, 6.5, 2.0, 3.2, 4.5, 6.0$.

It can be seen that the reconstruction is satisfactory. This means that, using the technique of combining several CB 's, the theoretical formulas provide good reconstructions.

We give the indicator value distribution in Figure 4.6 for all directions t with different l at each direction. We can see how the indicator near $t = 0.58\pi, \pi, 1.42\pi$ has some special property, which explains the difficulty of reconstructing these parts shown in Figures 4.4 and 4.5.

Next we consider Steps 2 and 3 by using (2.20) and (2.21), that is, we test the numerical behavior in distinguishing the boundary type and impedance in ∂D_I . Different from the formula (2.18), these two formulas need the boundary shape ∂D ,

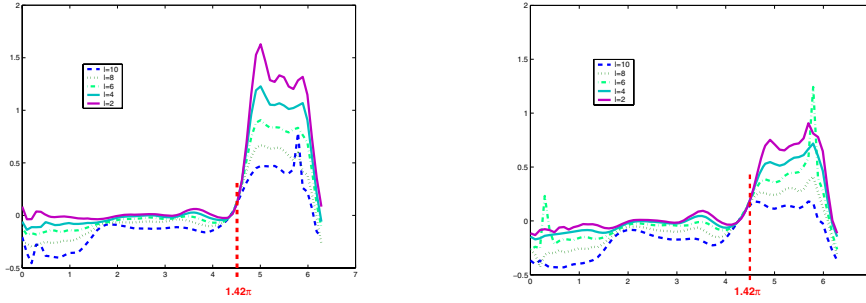


FIG. 4.7. Indicator values for different parts of the boundary using exact ∂D (left) and $\partial \tilde{D}$ with $\delta^* = 0.1$ (right).

which is theoretically obtained from (2.18). Since we can get some approximation to ∂D only numerically in terms of (2.18), it is necessary to check the approximate versions of (2.20) and (2.21) for distinguishing the boundary type and recovering $\sigma(x)$ on the coating part.

Step 2. We express the quantitative behavior for distinguishing ∂D_D and ∂D_I by giving the indicator distribution. As explained in Step 1, by using different blowup criteria in the shape reconstruction, we can get a good approximation to ∂D . In this step, we specify $\partial \tilde{D} \approx \partial D$ with an explicit expression given by

$$(4.4) \quad \partial \tilde{D} = \begin{pmatrix} \cos \delta^* & -\sin \delta^* \\ \sin \delta^* & \cos \delta^* \end{pmatrix} [\partial D + \{\delta^* \times (\cos t, \sin t) : t \in [0, 2\pi]\}]$$

with small constant $\delta^* > 0$, for simplicity. In this way, \tilde{D} is no longer symmetric with respect to x_1 , and the location for the corner part also differs from that of ∂D . To check the effect of this domain approximation on (2.20) and (2.21), we also evaluate them using the exact ∂D .

We generate $(\partial \tilde{D}_a^p, \partial D_a^p)$ from $(\partial \tilde{D}, \partial D)$ and therefore the sequences $(\{\tilde{z}_p\}, \{z_p\})$ as in (4.3). In this way, we have $\tilde{z}_p \rightarrow \tilde{a} \in \partial \tilde{D}$, $z_p \rightarrow a \in \partial D$, and $\delta_0, \delta_1 \rightarrow 0$. In the computation, we take $n = 32$ and decrease $\delta_0 = l \times 0.05 \rightarrow 0$ by taking l from 10 to 2. The indicator behavior using the same far-field pattern for ∂D and $\partial \tilde{D}$ with $\delta^* = 0.05$ is given in Figure 4.7.

Noticing the fact that the sound-soft part corresponds to the parameter $t \in [0, 1.42\pi]$, while the impedance part is related to $t \in [1.42\pi, 2\pi]$, the above numerical behavior supports (2.21) strongly with a large difference in $[0, 1.42\pi]$ and $[1.42\pi, 2\pi]$; that is, we can distinguish the boundary type in terms of the obvious difference of indicator values when z_p approaches the boundary (for small l), even if the boundary shape is known with a relative error.

Step 3. We compute the impedance coefficient on ∂D_I by applying the formulas for ∂D and also for its approximation $\partial \tilde{D}$. The reconstruction behavior for exact ∂D as well as its approximation $\partial \tilde{D}$ with $\delta^* = 0.05$ is shown in Figure 4.8. It can be seen that, for a given exact boundary shape ∂D , the theoretical result (2.21) for the impedance is valid (left figure), except near the end points of ∂D_I . The rough approximation in this part is reasonable, since this part is near to the sound-soft boundary. Using the approximate domain $\partial \tilde{D}$, the impedance can still be captured (right figure). Of course, the reconstruction is less accurate. Due to the nonconvex property of the obstacle and the mixed boundary condition, we think these results are satisfactory.

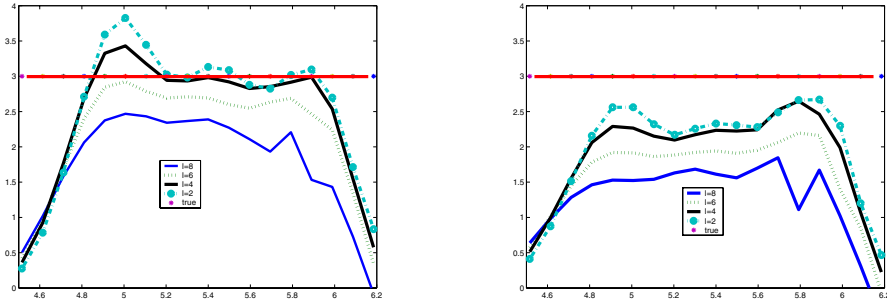


FIG. 4.8. Recovery of σ using exact ∂D (left) and approximate $\partial \tilde{D}$ with $\delta^* = 0.05$ (right).

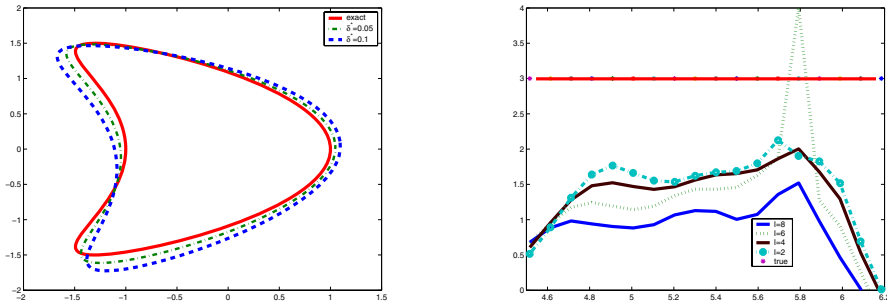


FIG. 4.9. Approximate $\partial \tilde{D}$ with $\delta^* = 0.05, 0.1$ (left) and reconstruction of σ for different l from approximate $\partial \tilde{D}$ with $\delta^* = 0.1$ (right).

However, if the perturbation for ∂D is very large, then the reconstruction of $\sigma(x(t))$ is much contaminated. This is due to the sensitivity of the approximate reconstruction to the boundary shape, especially for the corner part of the nonconvex domain, noticing that in the formula (2.21), the normal direction $\nu(a)$ appears. The perturbation scheme (4.4) moves the position of the corner part by rotation. An inversion result for the impedance with $\delta^* = 0.1$ is shown in Figure 4.9. From the left picture of this figure, we see how the corner part of $\partial \tilde{D}$ with $\delta^* = 0.1$ has been much moved from that of ∂D with a relative error almost 10%.

We conclude that the theoretical results (2.20) and (2.21) are well supported by our numerical tests even for nonconvex domains. If the approximate domain $\partial \tilde{D}$ is used in these two formulas, then we can still distinguish the boundary type in terms of the obvious blowup property of the indicator. However, the quantitative identification of impedance depends on the error level of ∂D .

Acknowledgments. The authors thank the anonymous referees for their valuable comments and suggestions, which led to a modified version of this paper.

REFERENCES

[1] I. AKDUMAN AND R. KRESS, *Direct and inverse scattering problems for inhomogeneous impedance cylinders of arbitrary shape*, Radio Sci., 38 (2003), pp. 1055–1064.
 [2] F. CAKONI AND D. COLTON, *The determination of the surface impedance of a partially coated obstacle from far field data*, SIAM J. Appl. Math., 64 (2004), pp. 709–723.
 [3] F. CAKONI, D. COLTON, AND P. MONK, *The determination of the surface conductivity of a partially coated dielectric*, SIAM J. Appl. Math., 65 (2005), pp. 767–789.

- [4] F. CAKONI AND D. COLTON, *Qualitative Methods in Inverse Scattering Theory*, Interaction of Mechanics and Mathematics, Springer, New York, 2006.
- [5] J. CHENG, J. J. LIU, G. NAKAMURA, AND S. Z. WANG, *Recovery of boundaries and types for multiple obstacles from the far-field pattern*, *Quart. Appl. Math.*, to appear.
- [6] J. CHENG, J. J. LIU, AND G. NAKAMURA, *Recovery of the shape of an obstacle and the boundary impedance from the far-field pattern*, *J. Math. Kyoto U.*, 43 (2003), pp. 165–186.
- [7] D. COLTON AND A. KIRSCH, *A simple method for solving inverse scattering problems in the resonance region*, *Inverse Problems*, 12 (1996), pp. 383–393.
- [8] D. COLTON AND R. KRESS, *Inverse Acoustic and Electromagnetic Scattering Theory*, 2nd ed., Springer, Berlin, 1998.
- [9] D. COLTON AND R. KRESS, *Integral Equation Methods in Scattering Theory*, John Wiley, New York, 1983.
- [10] D. J. HOPPE AND Y. RAHMAT-SAMII, *Impedance Boundary Condition in Electromagnetism*, Taylor and Francis, Oxford, UK, 1995.
- [11] N. HONDA, G. NAKAMURA, R. POTTHAST, AND M. SINI, *The no-response approach and its relation to non-iterative methods for the inverse scattering*, *Ann. Math. Pur. Appl.*, appeared online (DOI 10.1007/s10231-006-0030-1).
- [12] M. GRUTER AND K. O. WIDMAN, *The Green function for uniformly elliptic equations*, *Manuscripta Math.*, 37 (1982), pp. 303–342.
- [13] M. IKEHATA, *Reconstruction of the shape of the inclusion by boundary measurements*, *Comm. Partial Differential Equations*, 23 (1998), pp. 1459–1474.
- [14] M. IKEHATA, *Reconstruction of obstacles from boundary measurements*, *Wave Motion*, 3 (1999), pp. 205–223.
- [15] M. IKEHATA, *A new formulation of the probe method and related problems*, *Inverse Problems*, 21 (2005), pp. 413–426.
- [16] A. KIRSCH, *Characterization of the shape of a scattering obstacle using the spectral data of the far field operator*, *Inverse Problems*, 14 (1998), pp. 1489–1512.
- [17] R. KRESS AND W. RUNDELL, *Inverse scattering for shape and impedance*, *Inverse Problems*, 17 (2001), pp. 1075–1085.
- [18] W. LITTMAN, G. STANPACCHIA, AND H. F. WEINBERGER, *Regular points for elliptic equations with discontinuous coefficients*, *Ann. Scuola Norm. Sup. Pisa (III)*, 17 (1963), pp. 43–77.
- [19] G. NAKAMURA AND M. SINI, *Obstacle and boundary determination from scattering data*, *SIAM J. Math. Anal.*, to appear.
- [20] G. NAKAMURA, R. POTTHAST, AND M. SINI, *Unification of the probe and singular sources methods for the inverse boundary value problem by the no-response test*, *Comm. Partial Differential Equations*, 31 (2006), pp. 1505–1528.
- [21] R. POTTHAST, *Point Sources and Multipoles in Inverse Scattering Theory*, *Res. Notes Math.* 427, Chapman-Hall/CRC, Boca Raton, FL, 2001.
- [22] R. POTTHAST, *Sampling and probe methods—An algorithmical view*, *Computing*, 75 (2005), pp. 215–235.
- [23] R. POTTHAST, *A survey on sampling and probe methods for inverse problems*, *Inverse Problems*, 22 (2006), pp. R1–R47.
- [24] V. A. SOLONNIKOV, *On Green's matrices for elliptic boundary value problems (I)*, *Proc. Steklov. Inst. Math.*, 110 (1970), pp. 123–170.
- [25] V. A. SOLONNIKOV, *The Green's matrices for elliptic boundary value problems (II)*, in *Boundary Value Problems of Mathematical Physics*, *Proceedings of the Steklov Institute of Mathematics* 116, 1971, pp. 181–216; translated by the AMS, Providence, RI, 1973.